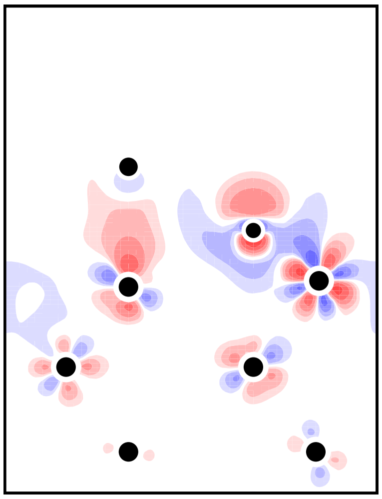

Figure 3.83: The change in the electron density due to the co-adsorption of cesium and oxygen to form the (2×2)-(1Cs+1O) structure

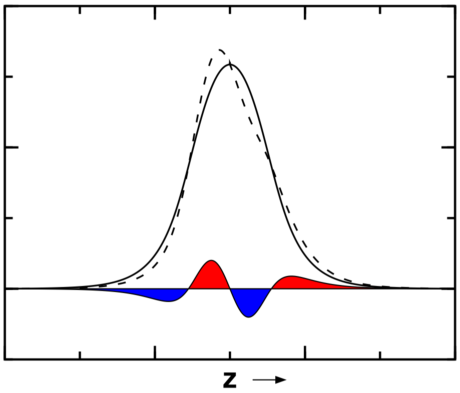

Figure 3.84: A schematic illustration of the change in the electron density on the vertical line passing through the centre of the oxygen atom due to the co-adsorption of cesium and oxygen to form the (2×2)-(1Cs+1O) structure

core region.

We further compare our results to the experimental images produced by the scanning tunnelling microscope; the measurements are from Trost (1995; Trost, Wintterlin & Ertl, 1995). In the Figures 3.85 and 3.86 we show the height maps of the constant density *i. e.* of a constant current within the Tersoff-Hamann model. The value of the density was chosen so that it reproduced the maximal corrugation from the experiments along a cut through the adsorbates. The Figure 3.87 can be compared to the measured images in the work of Trost (1995); the agreement is very good in both cases.

3.4.2 Co-adsorption of cesium and carbon monoxide

Also the co-adsorbed alkali metal and carbon monoxide mutually stabilise each other as was found in the thermal desorption spectroscopy for example in the case of K and CO on Ni (110) (Brodén, Gafner & Bonzel, 1979), Na, K and Cs with CO on Ni (100) (Kiskinova, 1981), and K and CO on Ru (0001) (Madey & Benndorf, 1985); an example of the thermal desorption spectra (Over *et al*, 1995b) is shown in the Figure 3.88 for Cs and CO on Ru (0001): whereas the desorption of Cs alone begins already at 450 K and the one of CO at 350 K, in the co-adsorbed layer the desorption does

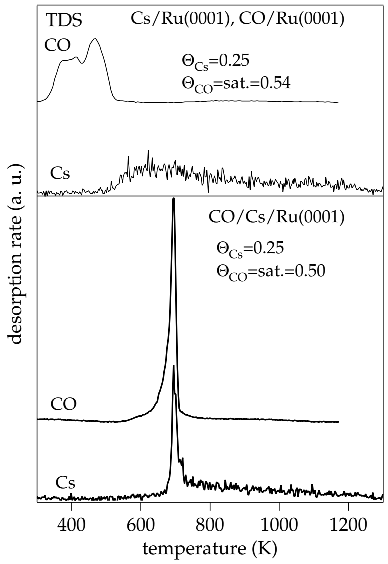

Figure 3.88: The thermal desorption spectra for cesium, carbon monoxide and the co-adsorbed phase on Ru (0001); from Over *et al* (1995b)

not begin until 650 K, and then the desorption occurs simultaneously.

The stabilisation of the co-adsorbates is due to an attractive interaction between the electro-positive alkali and the electro-negative carbon monoxide. The attraction has been concluded from the thermal desorption and vibrational spectra, since at low alkali coverages there appears two distinct states: In addition to the almost unchanged component and second one, with a higher desorption temperature and lower internal C-O stretching frequency. At low coverages of carbon monoxide only the second state, affected by the co-adsorbed alkali, is occupied, showing that it is the preferred adsorption state and thus a clustering of the co-adsorbates must take place; this implies that the adsorption is attractive. If the coverage of the alkali is large enough, all the carbon monoxide molecules must adsorb to sites at the vicinity of the alkali and are affected by it: only CO molecules in one state are thus observed. Due to the two different CO species, once the neighbourhood of the alkali has been filled, a short-range interaction between the alkali and CO was concluded, since the adsorption of further molecules is no longer significantly perturbed by the presence of the alkali on the surface.

The reduction of the C-O stretching frequency on all the systems studied so far points to a common mechanism in the co-adsorption systems. The usual interpretation is that the bond length of CO increases, yielding a lower frequency. In the few qualitative structural determinations up to date this has indeed been confirmed in the case of K and CO on Ni (111) (Davis *et al*, 1995; 1997), Cs and CO on Ru (0001) (Over *et al*, 1995b; 1995c), K and CO on Ru (0001) (Over *et al*, 1999), Na and CO on Pt (111) (Sette *et al*, 1985), and K and CO on Pt (111) (Moré, 1998). Simultaneously the size of the alkali metal atom is expected to decrease – *i. e.* the atom to move closer to the surface – since in the intuitive model the alkali acts as an electron donor, increasing the degree of ionisation when the CO is co-adsorbed because more of the charge from the *ns* state of the alkali would be transfered via the substrate to the partially empty, acceptor orbital $2\pi^*$ along the lines of the Blyholder model; the filling of this state, because anti-bonding and thus weakening for the internal C-O bond, also partially explains the lowering of the C-O vibrational frequency upon the co-adsorption of the alkali. The size of the alkali metal, characterised by its hard-ball radius, is however found to increase when CO is adsorbed, in contradiction with the simple charge-transfer model; in cases where the adsorption site of the alkali does not change this effect has so far been found in the systems Co (0001)-(2 × 2)-(K+2CO) (Lahtinen *et al*, 1998), Co (10$\bar{1}$0)-c(2 × 2)-(K+CO) (Kaukasoina *et al*, 1995), Ni (111)-(2×2)-(K+2CO) (Davis *et al*, 1995; 1997), Ru (0001)-(2×2)-(Cs+nCO), n=1,2 (Over *et al*, 1995b; 1995c) and Pt (111)-($\sqrt{3} \times \sqrt{3}$)-(K+CO) (Moré, 1998). In the case of Co (10$\bar{1}$0)-c(2 × 2)-(K+CO) the increase in the size of the potassium is extraordinarily large, 0.4 Å. The origin of the change of the size is still not understood.

Whereas the carbon monoxide alone adsorbs either on the three-fold hollow fcc – Ni (111) and Pd (111) – or on-top sites – Co (0001), Cu (111), Ru (0001), Rh (111) and Ir (111) on the trigonal surfaces, in the co-adsorbed phases with an alkali only three-fold adsorption sites have been found. Likewise although the alkali often adsorbs on a hollow site in the phase of a single adsorbate, in the co-adsorbate structure the alkali is exclusively found on the on-top site, with Pt (111) violating the rule. These effects point out to a general interaction mechanism in the mutual attraction between the ad-particles.

We studied the co-adsorption of cesium and carbon monoxide in the configurations with coverages equal to those which were solved experimentally using the low energy electron diffraction by Over *et al* (1995b; 1995c), namely Ru (0001)-(2 × 2)-(1Cs_{ot}+1CO_{hcp}) and Ru (0001)-(2 × 2)-(1Cs_{ot}+2$CO_{hcp,fcc}$); furthermore we calculated the structure Ru (0001)-(2 × 2)-(1Cs_{hcp}+1CO_{ot}), which is not experimentally observed but is instructive for studying why this structure is less stable than the Ru (0001)-(2 × 2)-(1Cs_{ot}+1CO_{hcp}). In addition to extract qualitative understanding of the nature of the effect of the alkali on the carbon monoxide we also studied the adsorption of CO alone but with an applied electric field, in the structures Ru (0001)-(2 × 2)-($CO_{ot}^{\mathbf{E}}$) Ru (0001)-(2 × 2)-($CO_{hcp}^{\mathbf{E}}$); the superscript **E** denotes the electric field. Similar density functional calculations on the poisoning and promotion upon co-adsorption were done by Mortensen *et al* (1998); however, their results cover a broader range and are more qualitative.

The geometries of our final geometries are compared in the Figure 3.89 and the Table 3.22 to the experimental observations, where possible. The C-O, Ru-C and co-adsorbate-to-nearest neighbour Ru bond lengths are also shown in the Table 3.23, where they are shown contrasted to the different chemical environment. Like in the experiments, the C-O bond length clearly increases relative to the isolated C-O phase from 1.15 Å to 1.26 Å by 0.11 Å, although in the experiments the change is only about 0.02 Å; however the error bars in the experimental analysis are large. The change in the bond length seems to consist of two origins:

- The change of adsorption site of the CO-only phase from on-top to hcp site accounts to 0.04 Å
- The co-adsorption of Cs when the molecule is on the hcp site causes the rest of the change, 0.07 Ä; this change can be understood as arising from the electric field created by the alkali. The magnitude of the electric field used in our calculation in the (2 × 2)-($CO_{ot}^{\mathbf{E}}$) system was only 0.6 eV/Å since at larger fields the slab becomes ionised; this value is, however, only one third or one quarter of the value felt by the CO in the case of co-adsorption with the alkali – please see the Section 3.3.1, and therefore we multiplied the change obtained, 0.02 Å, by a factor of three, where we have assumed that the change is almost linear with the applied field. The resulting change is 0.06 Å, very close to the change with the actual co-adsorption with the alkali metal

This observation that about 30-50 % of the change in the bond length is due to the site change and the rest from the field generated by the alkali is difficult to verify from the experimental observations

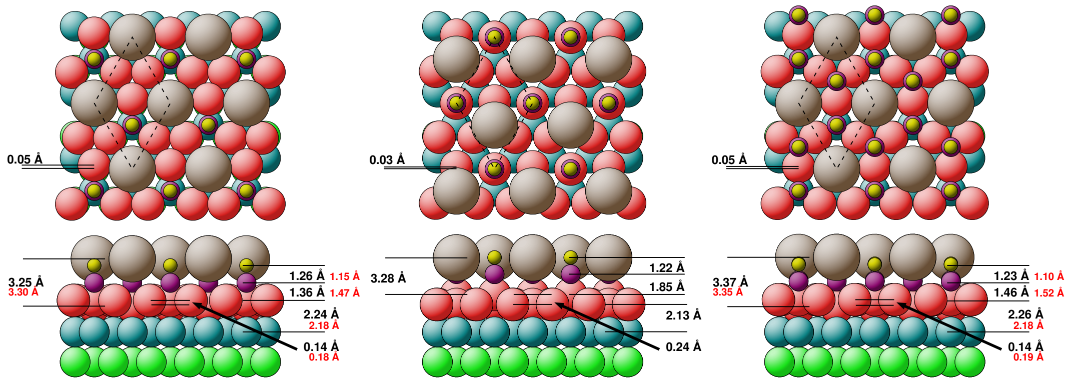

Figure 3.89: The geometries obtained from our calculations for the Cs+CO co-adsorption on Ru (0001); the experimental results by Over *et al* (1995b; 1995c) are denoted with a smaller font

due to the large error bars, which are often almost of the size of this effect. The changes of 0.05 Å for K+2CO/Ni (111), 0.07 Å for K+CO/Ru (0001) and 0.13 Å for K+CO/Pt (111) are similar in magnitude to our results, noting that there are two molecules per one alkali in the first structure, where CO adsorbs already on a three-fold hollow site in the isolated phase.

We made a further study on the effect of the electric field on the properties of an isolated CO molecule. This study we performed with a cluster program since we wanted too see the effect on the 1*s* states of carbon and oxygen. The results in the Table 3.24 suggest that in the electric field and charge state – please see below – which we have estimated to occur at the surface, namely $Z = -1.5$ electrons and 2.6 eV/Å, the change in the vibrational frequency, -143.6 meV from the free CO molecule agrees well with the experimental change of -141 meV, but the increase in the bond length 0.26 Å is much too large compared to the experimental value. However, the experimental results suffer from the large error bars and the shortening of the bond found recently (Over *et al*, 1995b; 1995c) is clearly not realistic. In our results we have not taken into account the screening and hybridisation of the molecular levels by the substrate and thus the eigenvalues in different charge states cannot be compared directly. The experiments of Strisland *et al* (1998) yield a reduction in the C and O 1*s* binding energies upon the co-adsorption of K to the CO/Rh (111) system, which is very similar to system in our study. Our values show a small increase, but we do not include any subtle many-body or final state effects present in the experiments, so a full comparison is not possible.

The Ru-C bond length can be seen to increase slightly with the electro-negativity of the co-adsorbate at the hcp site, but the change is much larger at the on-top site, achieving -0.10 Å. The Ru-C distance anti-correlates thus mostly with the C-O distance, whereas in the only experimental case to which we can compare, Ni (111), both C-O and Ru-C distances increase when the potassium is co-adsorbed (Schindler *et al*, 1993; Davis *et al*, 1995); at the corresponding coverage, $1\mathrm{Cs}_{\mathrm{ot}}$+$2\mathrm{CO}_{\mathrm{fcc,hcp}}$, a slight increase is seen also on the Ru (0001). Thus a general rule of the change in the Ru-C bond length might be difficult to achieve, also due to the small magnitude of the effect.

That the experimentally deduced interaction between the alkali metal and carbon monoxide is attractive is confirmed if the mixing energy

$$E_{\mathrm{mix}} = -E\,(\mathrm{Cs} + \mathrm{CO/Ru}) + E\,(\mathrm{CO/Ru}) + E\,(\mathrm{Cs/Ru}) - E\,(\mathrm{Ru}) \qquad (3.8)$$

is positive. In the configuration Ru (0001)-(2×2)-($\mathrm{Cs}_{\mathrm{ot}}$+$\mathrm{CO}_{\mathrm{hcp}}$) this energy is very large, -0.85 eV, and thus explains the clustering of alkali and carbon monoxide at low coverages and the large mutual

Table 3.22: The adsorption energy, change in work function, layer distances and distance of the cesium in the $(2 \times 2)°$-Cs_{ot}, cesium and carbon monoxide adsorbed on the Ru(0001) in the $(2 \times 2)°$-($1Cs_{ot}$+$1CO_{hcp}$) and $(2 \times 2)°$-($1Cs_{ot}$+$2CO_{hcp,fcc}$) structures, and the carbon monoxide adsorbed in the $(2 \times 2)°$-CO_{ot} from our density functional calculations. $E_{ads,Cs}$ and $E_{ads,CO}$ are the adsorption energies relative to a free cesium atom and carbon monoxide dimer, E_{mix} the mixing energy from the separated phases – Cs+CO and CO in the case of 1Cs+2CO – and $\Delta\phi$ the change in the work function from the clean surface; z_{12} is the average height between the first and second substrate layer, z_{C-Ru} and z_{Cs-Ru} the layer height from the nearest-neighbour atoms and d_{C-Ru} and d_{C-O} the corresponding distances

	Cs/Ru	CO/Cs/Ru	2CO/Cs/Ru	CO/Ru
$E_{ads,CO}$ (eV)	—	2.68	2.06	1.83
$E_{ads,Cs}$ (eV)	1.94	2.79	—	—
E_{mix} (eV)	—	0.85	0.26	—
$\Delta\phi$ (eV)	−3.44	−3.32	−2.74	+0.81
d_{C-Ru} (Å)	—	2.14	2.17, 2.17	1.93
d_{C-O} (Å)	—	1.26	1.23, 1.23	1.16
z_{Cs-Ru} (Å)	3.16	3.25	3.37	—
z_{C-Ru} (Å)	—	1.36	1.42, 1.49	1.93
z_{12} (Å)	2.15	2.20	2.21	2.16
b (Å)	0.03	0.14	0.18	0.17
Δx (Å)	+0.01	+0.05	+0.03	+0.01

Table 3.23: The distances and peaks in the density of states projected to the atomic orbitals in systems containing carbon monoxide in the (2×2)-(A+CO), A = co-adsorbate, structures from our density functional calculations; the second column from right is the peak due to the 2*s* level of oxygen or 5*s* level of cesium depending on which one is present on the surface in the structure

	d_{C-O} (Å)	d_{C-Ru} (Å)	d_{A-Ru} (Å)	$\bar{\varepsilon}_{CO,3\sigma}$	$\bar{\varepsilon}_{CO,4\sigma}$	$\bar{\varepsilon}_{CO,1\pi}$	$\bar{\varepsilon}_{CO,5\sigma}$	$\bar{\varepsilon}_{O,2s}$ / $\bar{\varepsilon}_{Cs,5s}$	$\bar{\varepsilon}_{Cs,5p}$
CO^{E}_{hcp}/Ru	1.21	2.16	—	−22.1	−9.7	−6.0	−6.6	—	—
Cs_{ot}/Ru	—	—	3.16	—	—	—	—	−23.1	−10.0
CO_{hcp}/Cs_{ot}/Ru	1.26	2.14	3.25	−21.8	−10.1	−6.0	−6.8	−22.5	−9.4
$2CO_{hcp,fcc}$/Cs_{ot}/Ru	1.23	2.17	3.37	−22.0	−9.9	−6.0	−6.9	−22.4	−8.9
CO_{hcp}	1.19	2.16	—	−22.3	−9.6	−6.0	−6.4	—	—
CO^{E}_{ot}	1.18	1.90	—	−23.3	−9.0	−6.4	−6.8	—	—
Cs_{hcp}/Ru	—	—	3.52	—	—	—	—	−23.0	−9.9
CO_{ot}/Cs_{hcp}/Ru	1.22	1.85	3.67	−23.5	−10.2	−6.8	−7.2	−23.5	−9.7
CO_{ot}	1.16	1.92	—	−23.3	−9.0	−6.2	−6.6	—	—
CO_{ot}/O_{hcp}/Ru	1.15	1.95	2.07	−23.4	−9.0	−6.3	−6.6	−19.0	—
CO_{ot}/$2O_{hcp,fcc}$/Ru	1.15	1.97	2.11	−23.4	−8.9	−6.3	−6.5	−18.5	—
O_{hcp}/Ru	—	—	2.07	—	—	—	—	−19.0	—

Table 3.24: The properties of a CO molecule in an applied electric field and in different charge states; calculated using an all-electron cluster code. The results for the neutral molecule in no field are shown as absolute, the other entries are changes relative to this configuration

Charge	$\lvert\mathbf{E}\rvert$ (eV/Å)	d_{C-O} (Å)	$\varepsilon_{1\sigma}$ (eV)	$\varepsilon_{2\sigma}$ (eV)	$\varepsilon_{3\sigma}$ (eV)	$\varepsilon_{4\sigma}$ (eV)	$\varepsilon_{1\pi}$ (eV)	$\varepsilon_{5\sigma}$ (eV)	$\varepsilon_{2\pi}$ (eV)	D (Debye)	ω (meV)
0.0	0.0	1.14	−515.2	−272.9	−29.2	−14.2	−11.8	−9.1	−2.1	+0.12	266.2
0.0	2.6	0.02	−0.1	−0.1	0.2	−0.6	0.0	1.1	0.4	1.7	−21.4
−0.8	0.0	0.08	8.2	8.1	9.1	7.6	8.3	7.5	6.7	1.0	−54.5
−0.8	2.6	0.13	8.1	8.5	9.7	7.2	8.6	8.6	7.3	1.4	−85.2
−1.5	0.0	0.17	14.6	14.2	16.6	13.8	15.1	13.5	12.1	2.0	−102.4
−1.5	2.6	0.26	14.4	14.9	17.6	13.7	15.5	14.5	12.6	1.4	−143.6

stabilisation. We can make an estimate on how much the desorption temperature should change if the pre-factor would not change; we recognise that this might be a drastic approximation and can justify it only *a posteriori*. If we however make the assumption, the change in the desorption energy is only due to the change in the activation energy for desorption, and since

$$e^{-E_a/(k_BT)} = e^{-E'_a/(k_BT')} = \text{constant} \ , \tag{3.9}$$

where E'_a is the activation energy in the presence of the co-adsorbate; then $T' = T \times E'_a/E_a$. As estimates for the activation energies of the isolated phases we use the binding energy, thus $E_a[(2\times2){-}\mathrm{Cs}] = 1.94$ eV, $E'_a[(2\times2){-}\mathrm{Cs}] = E_a[(2\times2){-}\mathrm{Cs}]+E_\mathrm{mixing} = 1.94+0.85 = 2.79$ eV, $E_a[(\sqrt{3}\times\sqrt{3})\mathrm{R}30^\circ{-}\mathrm{CO}] = 1.83$ eV and $E'_a[(\sqrt{3}\times\sqrt{3})\mathrm{R}30^\circ{-}\mathrm{CO}] = E_a[(\sqrt{3}\times\sqrt{3})\mathrm{R}30^\circ{-}\mathrm{CO}]+E_\mathrm{mixing} = 1.83+0.85 = 2.68$ eV. If we use as the corresponding temperatures where significant amount of desorption occurs $T[(2\times2){-}\mathrm{Cs}] \approx 500$ K and $T[(\sqrt{3}\times\sqrt{3})\mathrm{R}30^\circ - \mathrm{CO}] = 440$ K, we obtain

$$T'[(2\times2) - \mathrm{Cs}] \approx 720 \text{ K} \tag{3.10}$$

$$T'[(\sqrt{3}\times\sqrt{3})\mathrm{R}30^\circ - \mathrm{CO}] = 640 \text{ K} \ . \tag{3.11}$$

Since the latter one is lower it would be limiting the desorption; it is in surprisingly good value of the temperature 660 K where the desorption indeed occurs in the experiments of Over *et al* (1995b), giving further reliability to our calculated values for the adsorption and mixing energies.

Next we come to study in detail the electronic structure of the co-adsorption phase, and start with the density differences in the Figure 3.90; we show both the changes induced by adsorption of either adsorbate and the interaction density. Upon the adsorption of cesium to the surface pre-covered with CO the changes around the site of the alkali itself and at the substrate are very similar to the change by adsorption of cesium to the plane surface in the Figure 3.26; the form of the change at the CO site will be discussed soon below. When the carbon monoxide is adsorbed the change is again almost identical as when adsorbing on the clean surface around the molecule, but small around the cesium and rather opposite to the change when cesium was adsorbed. These changes are carried over into the interaction density in the right-most panel in the Figure 3.90: The changes at the near vicinity of the cesium are small and opposite to the changes when cesium adsorbs on the surface alone, and the change at carbon monoxide consists of a polarisation where the charge from carbon flows to oxygen; furthermore the ruthenium atoms of the top-most layer polarise, in the same direction as when cesium adsorbs on the clean surface. Thus the carbon monoxide induces

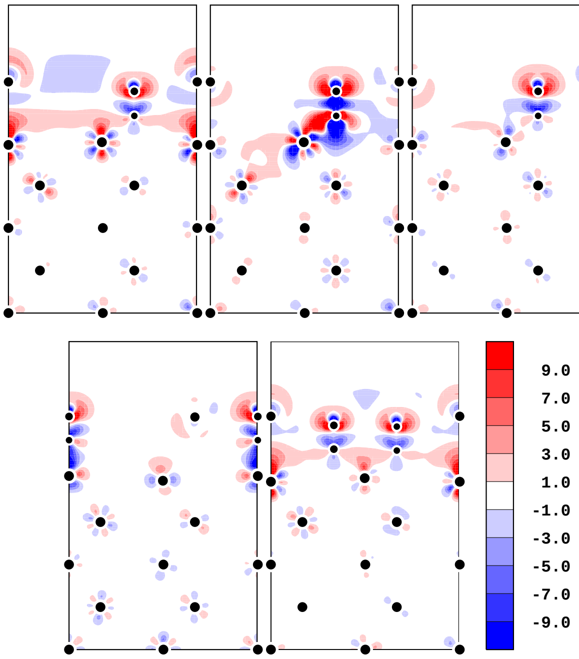

Figure 3.90: The change in the electron density obtained from our calculations upon the Cs+CO co-adsorption on Ru (0001). The upper panels from left to right: the change due to adsorption of cesium, due to carbon monoxide, and the interaction density in the Ru (0001)-(2×2)-(Cs_{ot}+CO_{hcp}) structure; the lower panels: the interaction density in the Ru (0001)-(2×2)-(Cs_{hcp}+CO_{ot} structure – left – and the change in the electron density due to the adsorption of cesium in the Ru (0001)-(2×2)-($1Cs_{ot}$+$2CO_{hcp,fcc}$) structure – right

a further polarisation of the surface, although the CO could also be expected to de-screen partially the polarisation of the surface atoms caused by the alkali.

The inner polarisation due to the co-adsorbed alkali is the most significant change in the electron density and seems to contradict the simple picture, based on the Blyholder model, that the co-adsorption of cesium should increase the occupation of the $2\pi^*$ orbital of CO. As will be shown below the occupation indeed does increase, but the change is rather small, only 15 % from the occupation of the value of CO adsorbed alone on the hcp site. Compared to the CO on the on-top site the change is, however, almost 70 %. This is the weak point of the interaction density: the constituent adsorbates are forced to the sites in the co-adsorbate structure instead of the equilibrium sites of the separated phases. We continue to analyse the interaction density since it gives valuable information on the characteristics of the interaction between the alkali and CO.

In order to pin-point the origins of the details in the density changes we study in which energy regions the changes occur. Therefore in the Figure 3.91 we plot the interaction density arising from different energy regions. What surprises most in the figure is that there is hardly no net gain visible in the energy region $E_F - 4$ eV< $E < E_F$, where the bonding hybrids of $2\pi^*$ orbitals should be located. Rather the increase in the density comes from the energy region $E_F - 20 < E < E_F - 5$ eV where the other molecular orbitals of CO are located. However the choice of the energy ranges modifies the plot somewhat, and a unique interpretation might be more involved than what is presented here.

It is instructive to compare the change in the electron density of the carbon monoxide due to the co-adsorption with an alkali metal to the change induced by an electric field only. This is shown in the Figure 3.92, and qualitatively the change is almost identical at the carbon monoxide; the

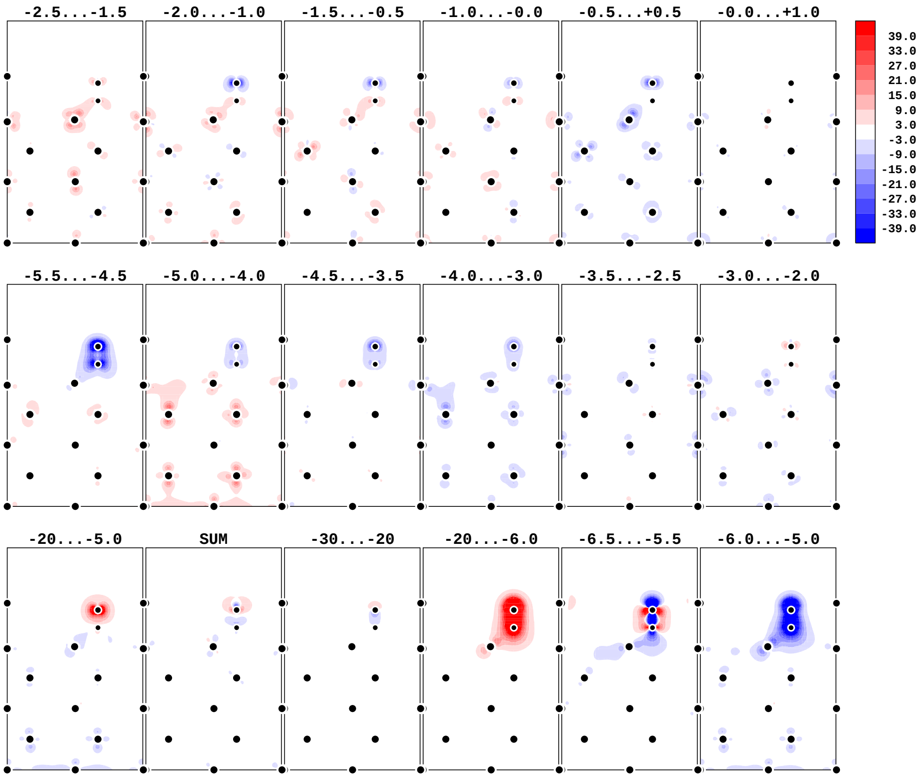

Figure 3.91: The interaction density in different energy regions obtained from our calculations for the Cs+CO/Ru co-adsorbed system; the energy regions are given in electron volts with respect to the Fermi energy. Please note that the region $E_F - 20$ eV... $E_F - 5.5$ eV has been summed in the left bottom corner as the states at the carbon monoxide switch the energy regions and thus make the comparison otherwise difficult

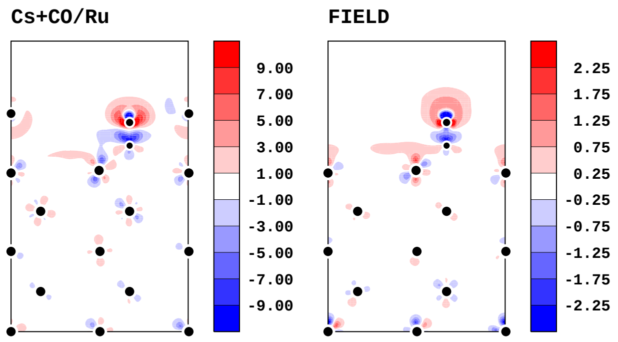

Figure 3.92: The change in the electron density obtained from our calculations for the Cs+CO/Ru co-adsorbed system; left is the interaction density and right the change in electron density due to an electric field of 0.6 eV/Å applied to CO adsorbed on the Ru (0001)

nearest-neighbour ruthenium atom has a polarisation of different sign though. Unfortunately we cannot apply a field whose magnitude would be comparable in magnitude to the one arising from the alkali metal. However, already this figure is convincing enough to allow the assignment of the major electronic effect of the cesium – beyond the induced site change – to be due to the induced electric field.

The change in the electron density along the surface normal gives insight into the formation and change of surface dipoles. The Figure 3.93 shows the change in the density both averaged perpendicular to the normal of the surface and two lines intersecting the adsorption sites of cesium and one of the three other, equivalent ruthenium atoms. The average change reduces further above the cesium atom from the value of cesium-covered surface only; this might be related to why the work function initially decreases when CO is adsorbed on the surface covered with alkali as found by Weimer, Umbach and Menzel (1985) for K+CO/Ru (0001). However, the internal polarisation of CO tends to increase the surface dipole since the charge is moved from carbon towards the oxygen. The density along the line through the centre of cesium shows the same interesting fact as the density differences in the Figure 3.90 that the density increases somewhat above the cesium atom; furthermore the density is almost independent of the co-adsorbates. Along the other line, passing through the three equivalent ruthenium atoms of the surface layer, the density just above and below shows an increase due to the filled d_{z^2} orbitals, but further away from the surface there is a depletion of charge density from the long-range 6s orbital of cesium.

The work function in the co-adsorbate phase 1Cs+1CO has increased by 0.1 eV compared to the Cs-only surface, and already by 0.7 eV in the phase 1Cs+2CO. These values are rather small compared to the increase caused by CO alone on the surface, 0.6 eV in the (2×2)-1CO cell, although the density is more polarised away from the surface when co-adsorbing with cesium and thus straight-forwardly thinking the work function should increase stronger.

It is difficult to learn about the electronic structure around the cesium atom by studying the radial electron density in the Figure 3.94 since it is very similar in all the cases studied here; it's not until the density of ruthenium or co-adsorbate atoms starts to contribute that differences occur. Therefore we rather study the asymptotic density above the cesium like was done in the case of adsorption of cesium alone in the Section 3.3.1. The results of the calculations in the Figure 3.95 illustrate basically two different kind of asymptotic densities: those in (3×3)-$\mathrm{Cs_{hcp}}$, (2×2)-($\mathrm{Cs_{ot}}$+$\mathrm{CO_{hcp}}$) and (2×2)-(1$\mathrm{Cs_{ot}}$+2$\mathrm{CO_{hcp,fcc}}$), and on the other hand in (2×2)-$\mathrm{Cs_{ot}}$ and (2×2)-($\mathrm{Cs_{ot}}$+$\mathrm{O_{hcp}}$). That the CO seems to decrease the density from the Cs_{6s} orbital more than the oxygen

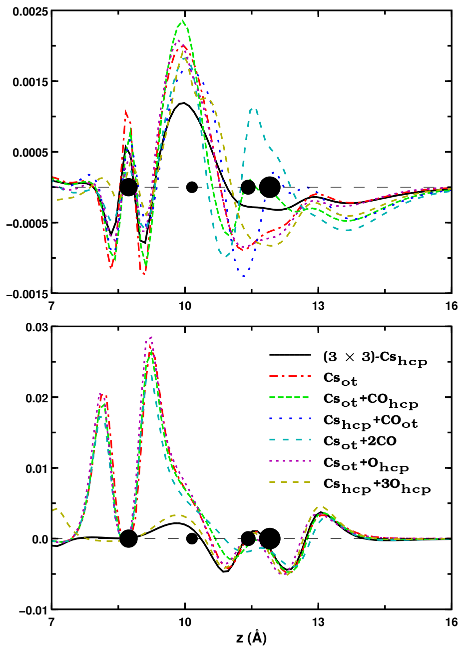

Figure 3.93: The change in the electron density averaged parallel to the surface – top panel – upon the adsorption of cesium onto the clean Ru (0001) and the surface covered with one and two carbon monoxide molecules or one and three oxygen atoms from our density functional calculations; also the changes along the surface line passing through the centre of the cesium – bottom panel – are shown. The atomic positions from the structure (2×2)-(Cs$_{ot}$-CO$_{hcp}$) are shown with filled circles of growing radii in the order carbon, oxygen, ruthenium and cesium. The positions are very similar also in the other structures; the oxygen atoms adsorb at a height close to that of carbon atom in the carbon monoxide. The unit cell is (2×2) except in the (3×3)-Cs$_{hcp}$ structure indicated

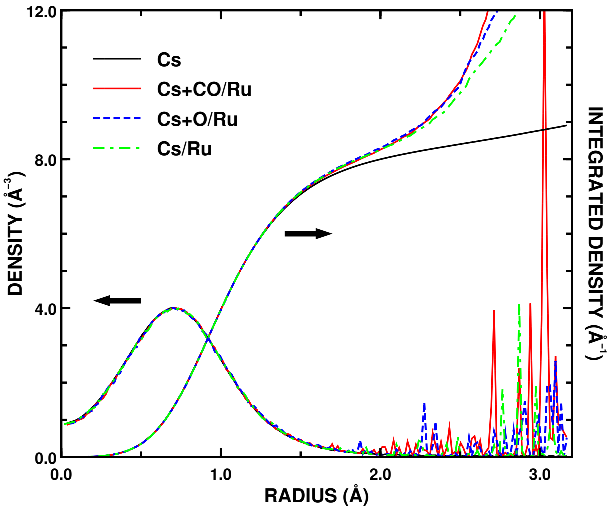

Figure 3.94: The density around the cesium atom in different structures: Free atom, Ru (0001)-(2 × 2)-(Cs_{ot}-CO_{hcp}), Ru (0001)-(2 × 2)-(Cs_{ot}-O_{hcp}) and Ru (0001)-(2 × 2)-Cs_{ot} and the integrated density; the scatter at large distances is due to the entrance of the density from the other atoms and is different in different directions. The numerical scale on both vertical axis is the same

atoms, even when the oxygen coverage is 3/4, is consistent with the results of meta-stable de-excitation spectroscopy measurements by Over *et al* (Fichtner-Endruschat *et al*, 1998; Herbert Over, personal communication, 1998). This difference between oxygen and carbon monoxide can also be seen in the change in the electron density around the Fermi energy in the Figure 3.96: Whereas the oxygen causes an increase above most of the surface the carbon monoxide causes a decrease. Thus from the calculated density changes the signal in the meta-stable de-excitation spectra from the cesium should be enhanced if oxygen is co-adsorbed and reduced if carbon monoxide is dosed onto the surface, exactly like seen in the experiments.

The densities of states projected onto the atomic states of the carbon atom of the carbon monoxide, onto the molecular orbitals of the carbon monoxide and onto the atomic 5*p* and 6*s* states of the cesium atom are shown in the Figures 3.97, 3.98 and 3.99, respectively, and the integrated densities of states are in the Tables 3.25 and 3.26. The energy-resolved curves can more conveniently be used to study the position of peaks and the integrated values the amount of different orbital characters.

The most notable qualitative feature in the states localised at the carbon monoxide – mainly the 3σ and the energy difference between the 5σ and 1π – is that they are almost insensitive to co-adsorbates and thus the only significant factor determining the position of these peaks is the adsorption site of the carbon monoxide; however the structure (2 × 2)-(Cs_{hcp}+CO_{ot}) forms an exception. The position of the 4σ level is not affected by the co-adsorbed oxygen, but the cesium causes a shift to energy close to that found at the hcp site, where the cesium does not change it. This contradicts the conclusion derived from the experimental results by Strisland *et al* (1998) who stated that the position of the peaks would be determined by the adsorption site only; however they could not be aware of the peak positions in the structure Cs_{hcp}+CO_{ot} since it is only metastable. For the other peaks their reasoning works. At the hcp site the Kohn-Sham eigenvalue of the 3σ state is at lower and that of 4σ at deeper binding energies, and the eigenvalue of the 5σ orbital becomes lower than of the 1π state, whereas at the on-top site the latter two peaks overlap almost exactly. Also the occupation of the $2\pi^*$ orbital is systematically larger when the CO is adsorbed at the hcp site, as

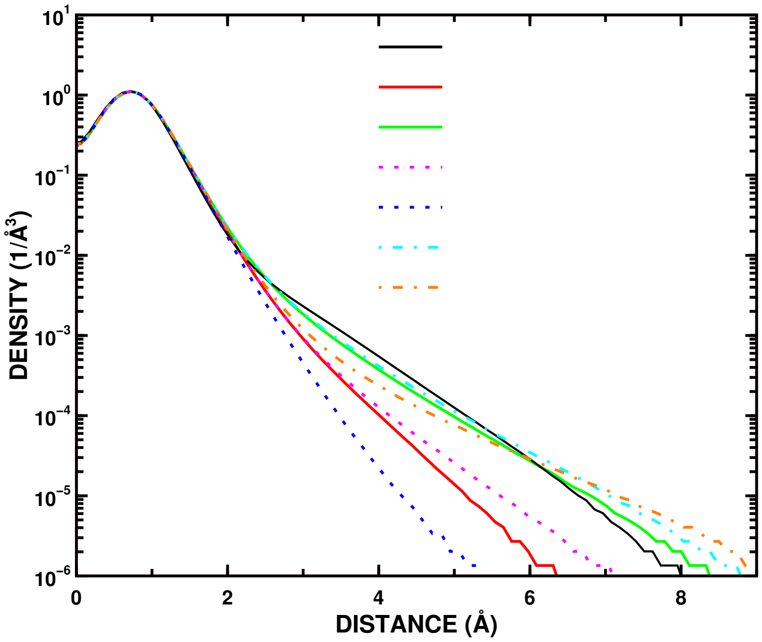

Figure 3.95: The asymptotic density above the cesium atom in different structures on the Ru (0001) surface as obtained from our calculations. The black line is the asymptotic density of a neutral cesium atom; the red, green, violet, blue, lila and orange lines are the densities in the (3×3)-Cs_{hcp}, (2×2)-Cs_{ot}, (2×2)-$(Cs_{ot}$+$CO_{hcp})$, (2×2)-$(1Cs_{ot}$+$2CO_{hcp,fcc})$, (2×2)-$(Cs_{ot}$+$O_{hcp})$ and (2×2)-$(1Cs_{hcp}$+$3O_{hcp})$ structures, respectively. Please notice that the structures with co-adsorbed CO are shown with short-dashed and the structures with co-adsorbed O with dot-dashed lines

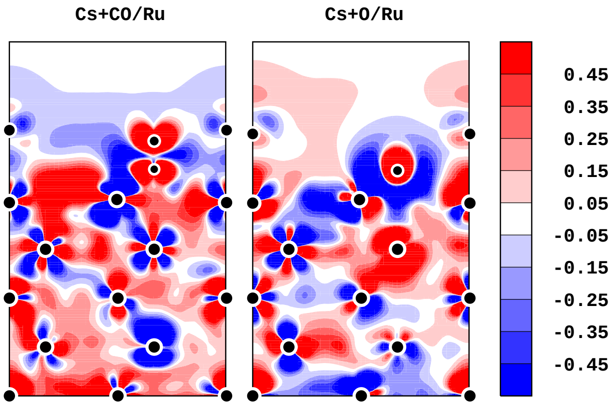

Figure 3.96: The induced density $\pm1/2$ eV around the Fermi energy due to the adsorption of carbon monoxide into the Ru (0001)-(2×2)-$(Cs_{ot}$-$CO_{hcp})$ – left – and oxygen into the Ru (0001)-(2×2)-$(Cs_{ot}$-$O_{hcp})$ – right – structure

well as the $4\sigma/5\sigma$ mixing. The "charge" at the CO molecule, obtained by summing up the integrals of the projections onto the molecular orbitals, shows a larger value at the hcp site, and as expected at the on-top site the charge decreases – along with an increase of the $4\sigma/5\sigma$ mixing – when the electro-negativity of the co-adsorbate increases. This is mainly due to the increased occupation of the $2\pi^*$ level; such a trend is in accord with the Blyholder model, although the change of the 5σ orbital is minimal. We warn, however, that the "charge" and orbital overlap should be regarded with some caution as the overlap in the adsorbed structure can also include some of the states of the substrate because the orthogonality between the substrate and molecular states does not hold when the hybrids have been formed.

The density of states projected at the atomic orbitals of the cesium atom reveals that the position of the semi-core $5s$ and $5p$ states shifts first upon its adsorption and further when co-adsorbates are added; the carbon monoxide increases the Kohn-Sham eigenvalues more than oxygen, and the more co-adsorbates the larger the increase. As was also seen in the Section 3.3.1 these eigenvalues are almost independent of the adsorption site, which is easily understandable due to the large distance of the cesium from the surface and the subsequent small corrugation and shallow site registry. The amount of $6s$ component of the states slightly reduces upon co-adsorption, and simultaneously the d states become increasingly occupied, especially the d_{z^2}. In the phases with the cesium co-adsorbed with carbon monoxide the $5s$ slightly hybridises with the energetically close-lying 3σ forming a bonding and an anti-bonding hybrids; however the amount of hybridisation is small as expected at such deep binding energies.

The structure with the two carbon monoxide molecules in the unit cell, Ru (0001)-(2×2)-($1Cs_{ot}$+$2CO_{hcp,fcc}$), behaves very similarly to the case of one molecule, yet the binding energy of the second molecule is naturally lower than of the first one but still more bound than in the adsorbed phase of the carbon monoxide alone; this demonstrates one cesium can easily bind two CO molecules as seen in the experiments. The work function raises further from the value of the alkali-covered surface, and the bond lengths d_{C-O} and d_{C-Ru} increase towards the value of the separated phase as the effect from the cesium has to divided up to the two molecules.

We shortly studied also the the bonding of the inverted molecule, *i. e.* with the oxygen towards to the surface, both with and without the co-adsorbed cesium. However, the molecule desorbed without even a local minimum from both the on-top and hcp sites from the Ru (0001)-(2 × 2)-OC geometry and the co-adsorbed Ru (0001)-(2 × 2)-(Cs_{ot}+OC_{hcp}) structure. Thus the possibility for a state with the rotated molecule as an intermediate in the oxidation reaction $^1/_2\,O_2$+CO→CO_2

3.4.3 Co-adsorption of oxygen and carbon monoxide

The co-adsorption of oxygen and carbon monoxide has not only interest because of the oxidation reaction but also since the real catalysts always contain oxygen. The oxidation rate has been shown to be enhanced by the sub-surface oxygen, first using catalysts in high pressures – please see *e. g.* the references in Peden (1992) or Rodriguez and Goodman (1991) – and later using quantitative single-crystal measurements in the ultra-high vacuum (Böttcher *et al*, 1997). We performed calculations only in the Ru (0001)-(2 × 2)-(CO_{ot}+O_{hcp}) co-adsorption structure shown in the Figure 3.101, and the Ru (0001)-(2 × 2)-($1CO_{ot}$+$2O_{hcp}$) – measured by Narloch, Held and Menzel (1994); the Ru (0001)-(2 × 2)-(2CO+1O) (Schiffer, Jakob & Menzel, 1997) has been realised in experiments but not calculated here. The relatively small repulsion between the adsorbed oxygen and carbon monoxide is

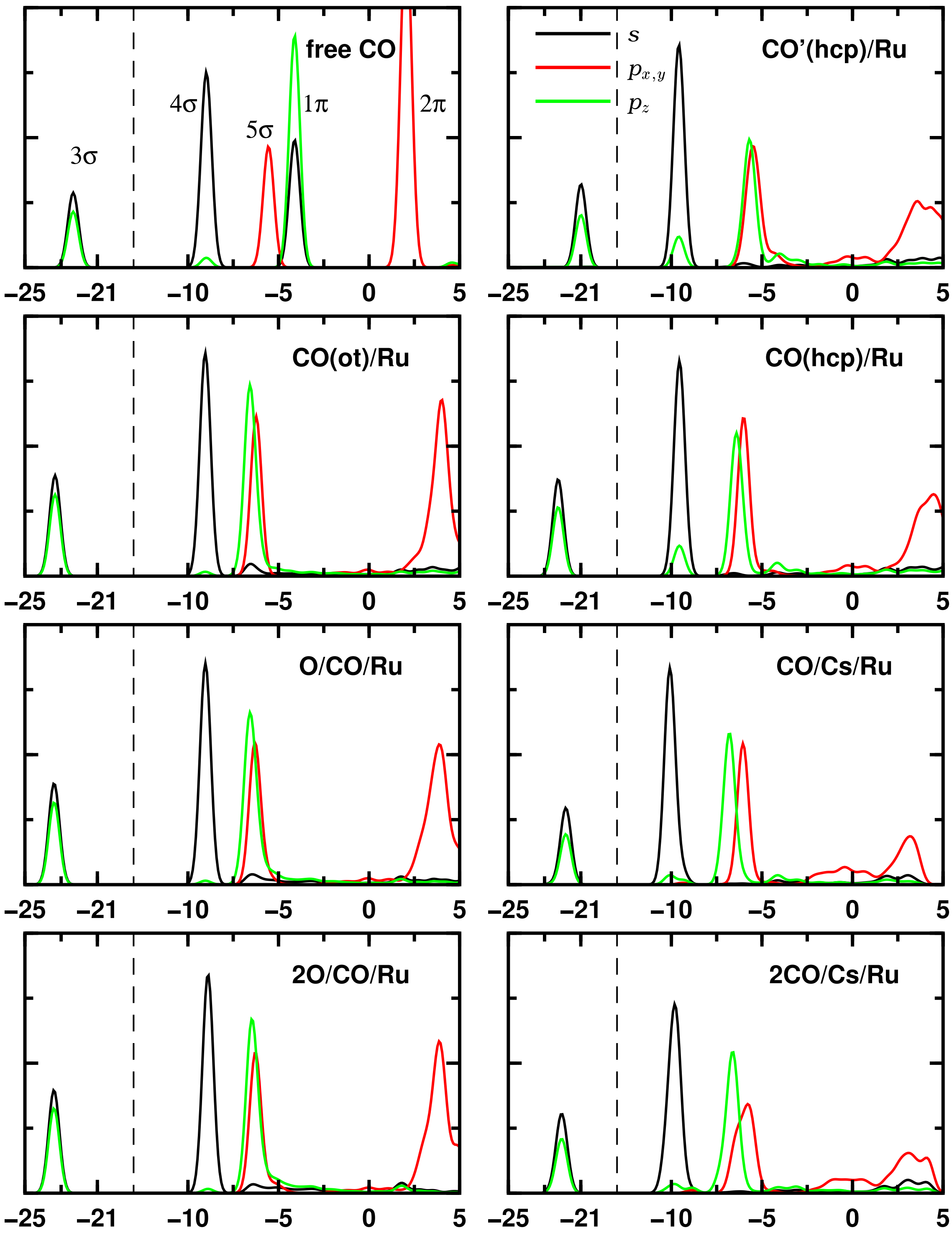

Figure 3.97: The density of states projected on the atomic orbitals of the carbon atom in different systems containing the carbon monoxide. "CO′(hcp)/Ru" refers to a CO molecule at hcp site with the geometry of the structure Ru-(2×2)-(Cs_{ot}+CO_{hcp}). The normalisation of the zero of energy is arbitrary in the case of the free molecule. The colours are s – black –, $p_{x,y}$ – red – and p_z – green

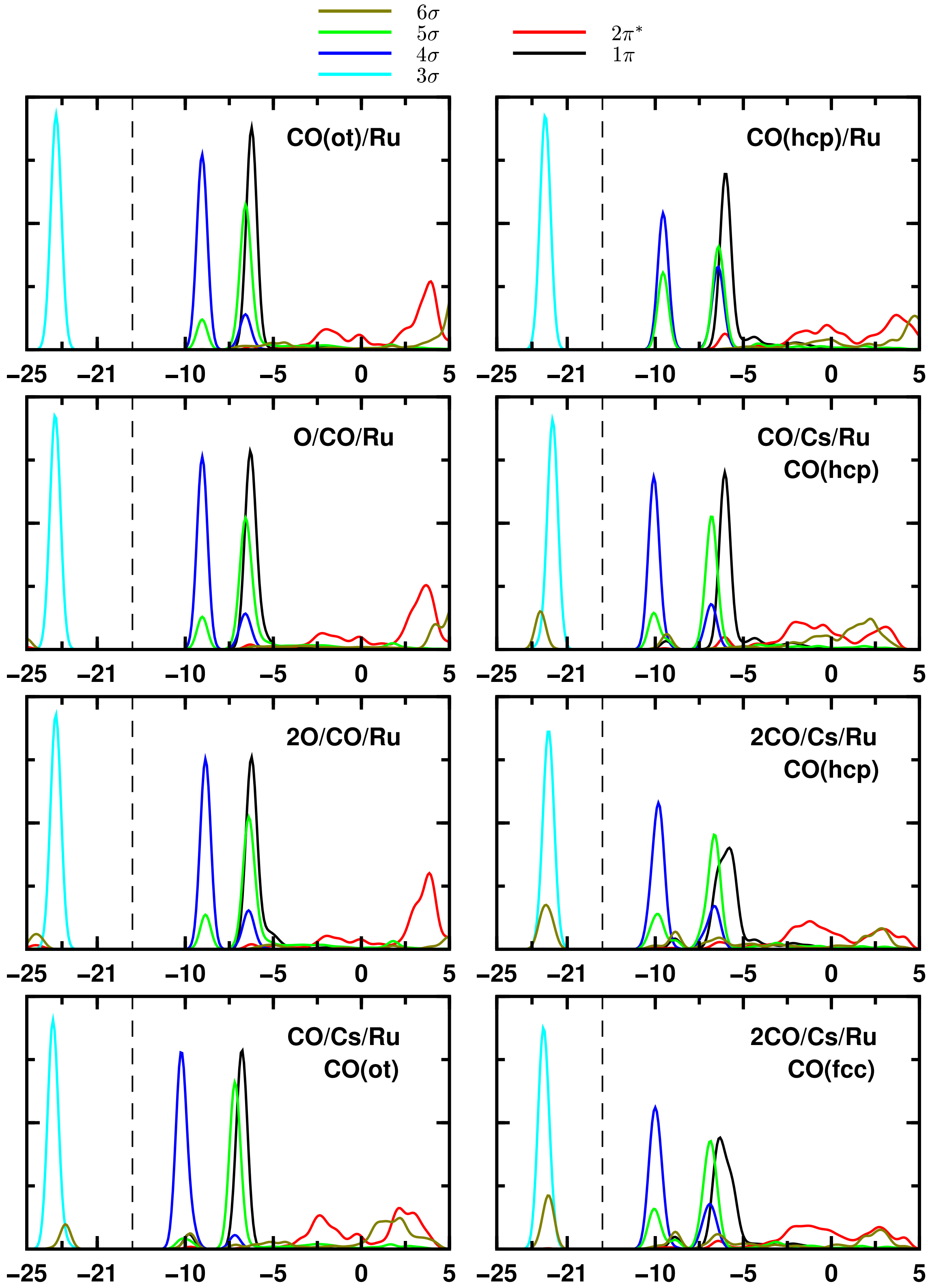

Figure 3.98: The density of states projected on the molecular orbitals of the carbon monoxide in different systems containing the molecule. The lines are lila – 3σ –, blue – 4σ –, green – 5σ –, brown – 6σ –, black – 1π – and red – 2π. The contributions of the π orbitals are symmetrised and halved

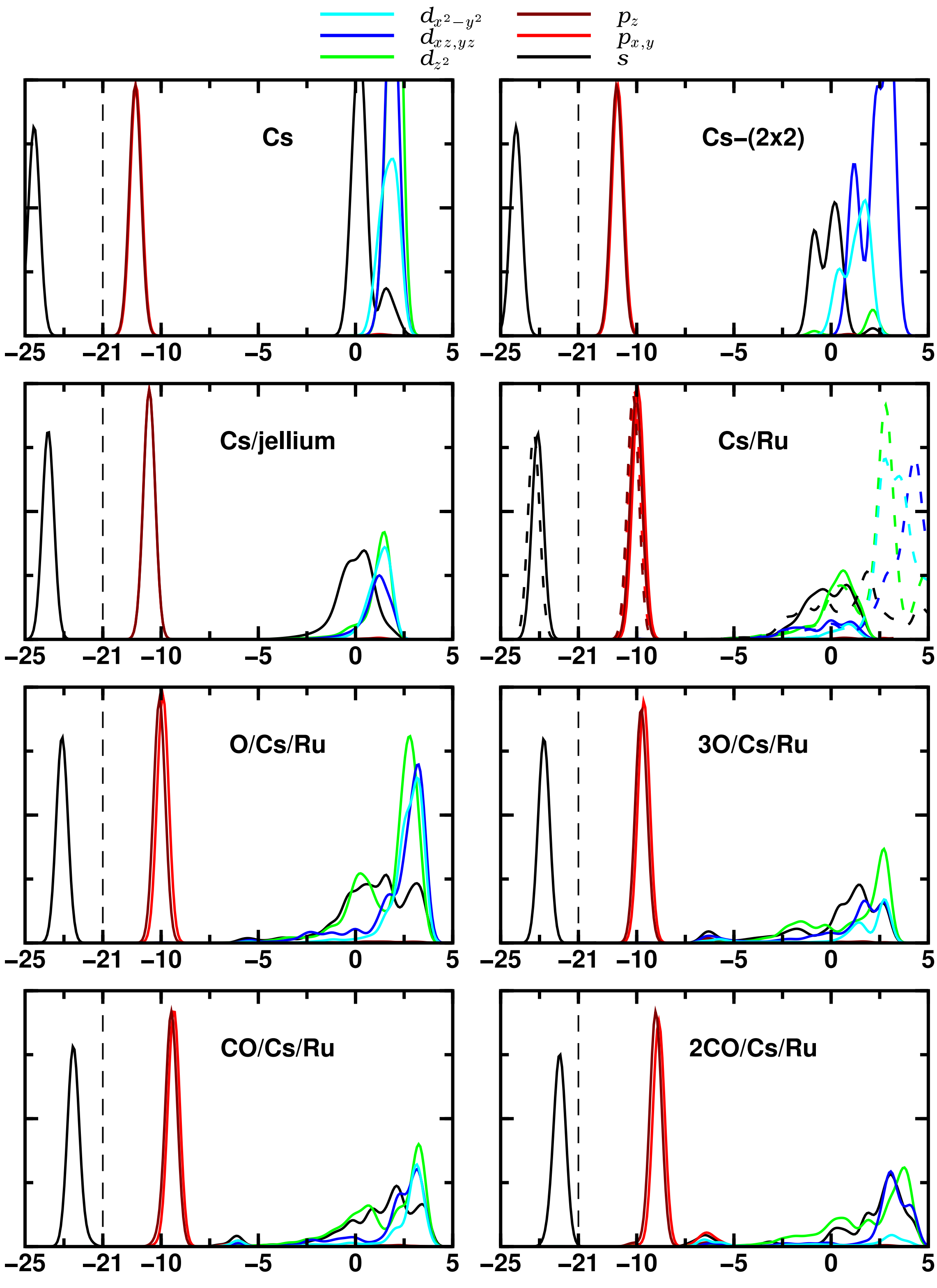

Figure 3.99: The density of states projected on the atomic orbitals of the cesium atom in different systems containing the cesium. The system "Cs" is a free atom in the (3×3) cell, "Cs-(2×2)" in the (2×2) cell. The system in "Cs/Ru" with the dashed lines is the cesium on ruthenium at the on-top site but in the geometry of the structure Ru-(2×2)-(Cs_{ot}+CO_{hcp}) but without the carbon monoxide; the system with solid line has been relaxed. The lines are black – s –, dark red – $p_{x,y}$ –, light red – p_z –, green – d_{z^2} –, blue – $d_{xz,yz}$ – and lila – $d_{x^2-y^2}$

Table 3.25: The integrals of the densities of states projected on the atomic orbitals. Ru_1 refers to the unique and Ru_2 to the three equivalent ruthenium atoms in the surface layer

Structure	Atom	s	$p_{x,y}$	p_z	d_{z^2}	$d_{xz,yz}$	$d_{x^2-y^2,xy}$
Ru (0001)-(2 × 2)-CO_{ot}	Ru_1	0.25	0.06	0.11	0.88	1.20	1.07
	Ru_2	0.24	0.06	0.04	1.06	1.20	1.07
	C	0.29	0.15	0.27			
	O	0.79	0.57	0.62			
Ru (0001)-(2 × 2)-CO_{hcp}	Ru_1	0.24	0.06	0.04	1.04	1.13	1.07
	Ru_2	0.24	0.07	0.05	1.09	1.10	1.07
	C	0.28	0.16	0.24			
	O	0.79	0.57	0.60			
Ru (0001)-(2 × 2)-(CO_{ot}+O_{hcp})	Ru_1	0.24	0.06	0.11	0.85	1.20	1.09
	Ru_2	0.24	0.07	0.05	1.10	1.08	1.07
	C	0.30	0.14	0.27			
	O	0.79	0.57	0.62			
	O	0.79	0.56	0.56			
Ru (0001)-(2 × 2)-(CO_{ot}+$2O_{hcp,fcc}$)	Ru_1	0.24	0.06	0.10	0.81	1.22	1.10
	Ru_2	0.23	0.07	0.07	1.10	1.05	1.08
	C	0.30	0.14	0.28			
	O	0.79	0.56	0.63			
	O	0.80	0.55	0.58			
	O	0.80	0.55	0.56			
Ru (0001)-(2 × 2)-Cs_{ot}	Ru_1	0.25	0.06	0.04	1.10	1.11	1.06
	Ru_2	0.24	0.06	0.04	1.09	1.10	1.06
	Cs	0.20	1.84	1.83	0.04	0.03	0.01
Ru (0001)-(2 × 2)-(Cs_{hcp}+CO_{ot})	Ru_1	0.25	0.07	0.11	0.93	1.14	1.10
	Ru_2	0.24	0.06	0.04	1.11	1.10	1.06
	Cs	0.16	1.85	1.84	0.04	0.02	0.01
	C	0.29	0.15	0.25			
	O	0.78	0.59	0.58			
Ru (0001)-(2 × 2)-(Cs_{ot}+CO_{hcp})	Ru_1	0.25	0.06	0.04	1.10	1.11	1.06
	Ru_2	0.24	0.07	0.05	1.12	1.08	1.07
	Cs	0.16	1.85	1.83	0.04	0.02	0.01
	C	0.27	0.17	0.22			
	O	0.78	0.60	0.56			
Ru (0001)-(2 × 2)-(Cs_{ot}+$2CO_{hcp,fcc}$)	Ru_1	0.25	0.07	0.04	1.11	1.11	1.06
	Ru_2	0.23	0.07	0.07	1.19	1.07	1.06
	Cs	0.15	1.86	1.84	0.03	0.01	0.01
	C_h	0.27	0.16	0.23			
	C_f	0.28	0.16	0.23			
	O_h	0.78	0.59	0.57			
	O_f	0.78	0.59	0.58			
Ru (0001)-(2 × 2)-(Cs_{ot}+O_{hcp})	Ru_1	0.25	0.07	0.04	1.11	1.10	1.08
	Ru_2	0.23	0.07	0.05	1.12	1.06	1.03
	Cs	0.18	1.85	1.83	0.05	0.03	0.01
	O	0.79	0.56	0.57			
Ru (0001)-(2 × 2)-($1Cs_{hcp}$+$3O_{hcp}$)	Ru_2	0.22	0.07	0.07	1.15	1.02	1.10
	Ru_1	0.22	0.08	0.09	1.22	0.94	1.12
	Cs	0.16	1.85	1.84	0.05	0.02	0.01
	O	0.79	0.56	0.56			

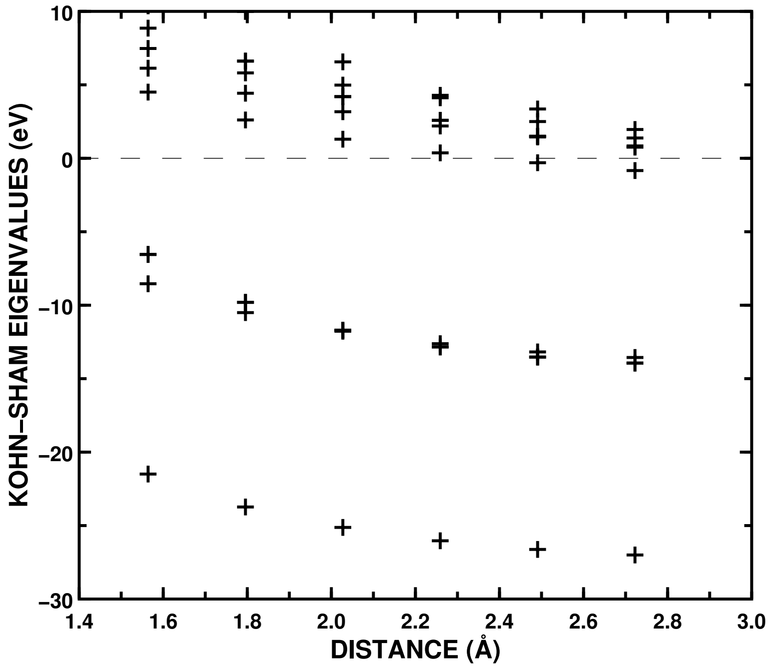

Figure 3.100: The Kohn-Sham eigen-values of a cesium atom in a hexagonal parallelepiped equivalent to the (2×2) cell used in the slab calculations. The free space between the atoms was reduced by applying a highly repulsive potential with the hexagonal shape. The zero of energy is set to the electro-static potential far away from the atom

Table 3.26: The occupation factors of different molecular levels of CO deduced from the projection of the Kohn-Sham states of the adsorption system on the molecular orbitals, and the mixing of 4σ and 5σ defined as the amount of molecular 5σ character of the 4σ in the adsorption system and vise versa

	Orbital						$4\sigma/5\sigma$	Charge
Structure	3σ	4σ	5σ	6σ	1π	$2\pi^*$	mixing (%)	at CO (e^-)
Ru (0001)-(2×2)-(Cs_{hcp}+CO_{ot})	0.998	0.988	0.883	0.062	0.969	0.350	5	−1.14
Ru (0001)-(2×2)-CO_{ot}	0.999	0.995	0.898	0.099	0.984	0.241	12	−0.88
Ru (0001)-(2×2)-(CO_{ot}+O_{hcp})	0.999	0.996	0.901	0.059	0.984	0.225	13	−0.75
Ru (0001)-(2×2)-(Cs_{ot}+CO_{hcp})	0.998	0.985	0.897	0.090	0.961	0.423	18	−1.48
Ru (0001)-(2×2)-CO_{hcp}	0.999	0.995	0.905	0.091	0.977	0.349	34	−1.28